Wagle, P., Zhang, Y., Jin, C., Xiao, X. (2016): Comparison of solar-induced chlorophyll fluorescence, light-use efficiency, and process-based GPP models in maize. - *Ecological Applications*, *26*, 4, pp. 1211—1222.

DOI: http://doi.org/10.1890/15-1434

Ecological Applications, 26(4), 2016, pp. 1211–1222

Comparison of solar-induced chlorophyll fluorescence, light-use efficiency, and process-based GPP models in maize

Pradeep Wagle,[1] Yongguang Zhang,[2,3,4,6] Cui Jin,[1] and Xiangming Xiao[1,5]

[1]*Department of Microbiology and Plant Biology, Centre for Spatial Analysis, University of Oklahoma, Norman, Oklahoma 73019 USA*
[2]*Jiangsu Provincial Key Laboratory of Geographic Information Science and Technology, International Institute for Earth System Sciences, Nanjing University, 210023 Nanjing, China*
[3]*Jiangsu Center for Collaborative Innovation in Geographical Information Resource Development and Application, 210023 Nanjing, China*
[4]*Remote Sensing Section, Helmholtz Center Potsdam, GFZ German Research Center for Geosciences, Telegrafenberg A17, 14473 Potsdam, Germany*
[5]*Insitute of Biodiversity Science, Fudan University, Shanghai, 200433 China*

Abstract. Accurately quantifying cropland gross primary production (GPP) is of great importance to monitor cropland status and carbon budgets. Satellite-based light-use efficiency (LUE) models and process-based terrestrial biosphere models (TBMs) have been widely used to quantify cropland GPP at different scales in past decades. However, model estimates of GPP are still subject to large uncertainties, especially for croplands. More recently, space-borne solar-induced chlorophyll fluorescence (SIF) has shown the ability to monitor photosynthesis from space, providing new insights into actual photosynthesis monitoring. In this study, we examined the potential of SIF data to describe maize phenology and evaluated three GPP modeling approaches (space-borne SIF retrievals, a LUE-based vegetation photosynthesis model [VPM], and a process-based soil canopy observation of photochemistry and energy flux [SCOPE] model constrained by SIF) at a maize (*Zea mays* L.) site in Mead, Nebraska, USA. The result shows that SIF captured the seasonal variations (particularly during the early and late growing season) of tower-derived GPP (GPP_EC) much better than did satellite-based vegetation indices (enhanced vegetation index [EVI] and land surface water index [LSWI]). Consequently, SIF was strongly correlated with GPP_EC than were EVI and LSWI. Evaluation of GPP estimates against GPP_EC during the growing season demonstrated that all three modeling approaches provided reasonable estimates of maize GPP, with Pearson's correlation coefficients (r) of 0.97, 0.94, and 0.93 for the SCOPE, VPM, and SIF models, respectively. The SCOPE model provided the best simulation of maize GPP when SIF observations were incorporated through optimizing the key parameter of maximum carboxylation capacity (V_{cmax}). Our results illustrate the potential of SIF data to offer an additional way to investigate the seasonality of photosynthetic activity, to constrain process-based models for improving GPP estimates, and to reasonably estimate GPP by integrating SIF and GPP_EC data without dependency on climate inputs and satellite-based vegetation indices.

Key words: *maize phenology; SCOPE; SIF; vegetation indices; VPM.*

Introduction

It is important to accurately estimate cropland gross primary production (GPP) due to its key role in the global food security and carbon budgets (Peters et al. 2007). In particular, the corn belt of the midwestern USA supplies 40% and 35% of global annual maize (*Zea mays* L.) and soybean (*Glycine max* L.) productions, respectively (FAO 2013), and thus plays an important role in the annual carbon balance of North America (Peters et al. 2007). Different approaches of GPP estimations have been developed in past decades. One main approach is the use of satellite-based production efficiency models (PEMs) that are developed based on the light-use efficiency (LUE) concept (Monteith 1972). Formulation of the LUE-based PEMs to estimate GPP is as follows:

$$\mathrm{GPR} = \mathrm{PAR} \times \mathrm{FPAR} \times \mathrm{LUE}, \quad (1)$$

where LUE is the efficiency with which the absorbed photosynthetically active radiation (PAR) is used in photosynthesis and FPAR is the fraction of absorbed PAR by vegetation. LUE is generally tabulated with invariant values associated to plant functional types, then attenuated by temperature and water stressors under limiting environmental conditions. An estimation of LUE from remote sensing is still challenging (Hilker

Manuscript received 3 August 2015; revised 19 October 2015; accepted 5 November 2015. Corresponding Editor: D. S. Schimel.
[6]E-mail: yongguang_zhang@nju.edu.cn

et al. 2008). FPAR is commonly approximated from remotely sensed vegetation indices. Based on different FPAR concepts, there are two typical groups of satellite-based LUE models. The first group uses the fraction of PAR absorbed by vegetation canopy ($FPAR_{canopy}$) to simulate GPP, which includes the Moderate-Resolution Imaging Spectroradiometer Photosynthesis (MODIS-PSN) model (Running et al. 2004), the eddy covariance-based LUE (EC-LUE) model (Yuan et al. 2007), and the Carnegie–Ames–Stanford Approach (CASA) model (Potter et al. 1993). $FPAR_{canopy}$ is often estimated from normalized difference vegetation index (NDVI) or leaf area index (LAI; Sellers et al. 1997). The second group uses the fraction of PAR absorbed by vegetation chlorophyll ($FPAR_{chl}$), which includes vegetation photosynthesis model (VPM; Xiao et al. 2004). Recently, several GPP models have either estimated $FPAR_{chl}$ from enhanced vegetation index (EVI) or considered EVI as a proxy of $FPAR_{chl}$ (Xiao et al. 2004, Wu et al. 2011). The VPM has been evaluated for maize (Kalfas et al. 2011) and soybean (Wagle et al. 2015) croplands, and showed an improvement on estimating GPP of croplands compared to the $FPAR_{canopy}$-based MODIS-PSN model. Even though the relatively simple LUE-based models have widely been used in estimating GPP at regional and global scales, their performance has been different (Jung et al. 2007, Nightingale et al. 2007) due to variations in model structures and parameters, and uncertainties of model inputs (Wang et al. 2011, Jin et al. 2015).

Another main approach to estimate GPP at different temporal and spatial scales is to use process-based terrestrial biosphere models (TBMs; Sellers et al. 1997). TBMs generally represent physiological, biophysical, and biogeochemical processes in a mechanistic way of photosynthesis, respiration, and canopy energy balance (Sellers et al. 1997), and they require more inputs, most importantly meteorological, soil, and land cover information. Most of these models rely on C_3 and C_4 photosynthesis models (Farquhar et al. 1980, Collatz et al. 1992) to estimate GPP. The soil canopy observation of photochemistry and energy flux (SCOPE) model belongs to this group and can be used to simulate carbon, water vapor, and heat fluxes (Van der Tol et al. 2009*a*).

It has recently been shown that space-borne sun-induced chlorophyll fluorescence (SIF) observations offer new possibilities for monitoring photosynthesis from space (Frankenberg et al. 2011, Guanter et al. 2014). Chlorophyll fluorescence is an electromagnetic emission in the 650–800 nm range originating at the core of photosynthetic machinery. The first global retrievals of SIF from the Greenhouse gases Observing SATellite (GOSAT; Frankenberg et al. 2011, Joiner et al. 2011, Guanter et al. 2012) and later from the Global Ozone Monitoring Experiment-2 (GOME-2; Joiner et al. 2013) enable the establishment of a direct link between remotely sensed SIF and GPP of terrestrial ecosystems. A recent empirical study showed the ability of space-borne SIF to monitor crop photosynthesis at regional and global scales and to correct existing underestimations by LUE models like MODIS-PSN (Guanter et al. 2014). Compared to reflectance-based satellite data (e.g., FPAR), Joiner et al. (2014) showed that SIF can track spring onset and autumn decline of photosynthesis more closely in different biomes. Zhang et al. (2014) demonstrated that key parameters for photosynthesis modeling, such as the maximum carboxylation capacity (V_{cmax}) can be derived from space-borne SIF data and the SCOPE model, which could improve GPP estimates. Similar to the fundamental estimation of GPP based on the LUE concept (Monteith 1972), SIF is conceptualized as (Guanter et al. 2014)

$$SIF = PAR \times FPAR \times LUF_f, \quad (2)$$

where LUE_f is the light-use efficiency for fluorescence. Obviously, both SIF and GPP are related to the flux of absorbed light (APAR or FPAR) with which it is used for vegetation photosynthesis.

Considering different concepts of FPAR ($FPAR_{canopy}$ and $FPAR_{chl}$), it is also necessary to perform an additional comparison of their relationships with space-borne SIF observations in order to quantify the link between fluorescence and vegetation photosynthesis process. As chlorophyll fluorescence is closely related to the photosynthetic activity of vegetation, we expect consistency of crop phenology in GPP and SIF. In the meanwhile, since SIF is an independent measurement, the link between SIF and APAR or FPAR can provide more insights into the usage of satellite-derived spectral vegetation indices as well. In addition, it is also useful to determine the usefulness of SIF relative to other commonly used vegetation indices such as land surface water index (LSWI) which has shown advantage for identifying the crop maturity date over NDVI and EVI (Yan et al. 2009).

To our knowledge, no simultaneous comparison of the performance of space-borne SIF in estimating GPP with the LUE-based VPM and process-based SCOPE models has been made in croplands. The major objectives of this study were to (1) investigate consistency of seasonal dynamics of maize phenology based on observations of carbon flux, vegetation indices, and SIF, and (2) compare the performance of SIF for estimating maize GPP with a LUE-based (VPM) and process-based (SCOPE) GPP models. Considering the large uncertainty in the magnitude of predicted GPP for croplands and substantial differences in the spatial and temporal variability of GPP by the models (Huntzinger et al. 2012, Schaefer et al. 2012), this type of simultaneous comparison study would improve our ability to accurately estimate GPP of croplands. The improved GPP estimation could not only benefit crop yield forecast for a wide range of public and private sectors, but also help better understanding the role of croplands in global carbon budgets and atmospheric CO_2 seasonal cycle (Peters et al. 2007, Gray et al. 2014, Zeng et al. 2014).

Materials and Methods

Site descriptions and flux data

Three AmeriFlux crop sites, located at the University of Nebraska-Lincoln Agricultural Research and Development Center near Mead, Nebraska, USA, were used in this study. Site 1 (USNe1) is irrigated continuous maize, and site 2 (USNe2) and site 3 (USNe3) are planted in maize-soybean rotations. The difference between USNe2 and USNe3 sites is the USNe2 site is irrigated and the USNe3 site is a rainfed agricultural system. Detailed site information can be found in previous studies (Verma et al. 2005, Suyker and Verma 2012). To determine landscape homogeneity of the study area, MODIS products for land cover type (MCD12C1; Friedl et al. 2010) and EVI (MOD13C2; Huete et al. 2002) with spatial resolution of 0.05 degrees were used. It was found that more than 90% of the GOME-2 pixel area around the Mead flux tower sites corresponded to croplands and the standard deviation of EVI was less than 0.1. Thus, we assumed landscape homogeneity within the GOME-2 grid, even though the footprint size of the flux tower (<1 km^2) does not match the coarse resolution of GOME-2. This assumption of landscape homogeneity could lead to biases to some extent in the comparison. However, using the same SIF and flux dataset, previous studies demonstrated good performance of this assumption (Guanter et al. 2014, Zhang et al. 2014).

Half-hourly carbon flux and meteorological data from three study sites for the period of 2007–2011 were obtained from the AmeriFlux website (*available online*).[7] We used flux data only for the maize growing years for USNe2 and USNe3 sites. Flux data were gap-filled and partitioned using the tool eddy covariance gap-filling and flux-partitioning tool from the Max Planck Institute for Biogeochemistry (MPI-BGC; *available online*).[8] The net ecosystem CO_2 exchange (NEE) was partitioned into GPP (GPP_EC) and ecosystem respiration (Reichstein et al. 2005).

GOME-2 SIF data

We used SIF data for the study period (2007–2011) from GOME-2 instrument onboard Eumetsat's MetOp-A platform. GOME-2 has a sun-synchronous orbit and samples near 09:30 local time. GOME-2 measures in the 240–790 nm spectral range with a relatively high spectral resolution between 0.2 and 0.5 nm and a nominal footprint of 40 × 80 km^2. SIF retrievals are based on the inversion of top-of-atmosphere measurements in the 715–758 nm windows that overlap SIF emission. The retrieval method disentangles the contribution of atmospheric absorption and scattering, surface reflectance, and fluorescence to the measured top-of-atmosphere radiance spectra. Details of the retrieval of SIF from GOME-2 measurements can be found in Joiner et al. (2013) in which an effective cloud fraction of <0.4 was used to filter and quality control. Details about the effects of cloud on fluorescence measurements can be found in previous studies (Joiner et al. 2013, 2014). The retrievals are quality-filtered and binned in 0.5° latitude–longitude grid boxes (Joiner et al. 2013).

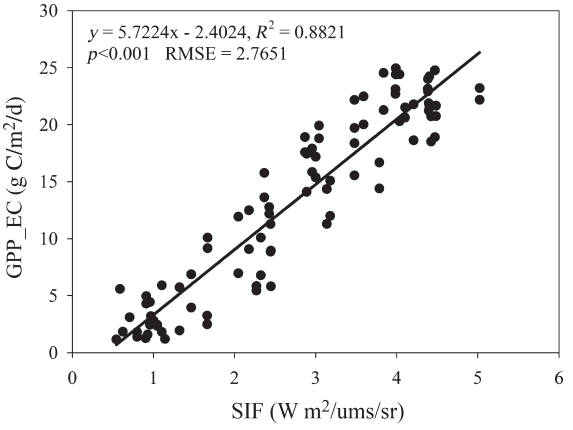

FIG. 1. A relationship between 8-d tower-based gross primary production (GPP_EC) and sun-induced chlorophyll inflorescence (SIF) during the maize growing season for two Mead rotation sites (USNe2 and USNe3).

Space-borne SIF values were extracted based on the coordinates of the flux tower and averaged to an 8-d period to match 8-d composites of MODIS data set, when at least five SIF retrievals were available within each 8-d period. Due to the coarse resolution of GOME-2 grid, we actually extracted the same SIF values for the three maize sites. GPP_EC data from USNe2 and USNe3 sites were used to derive an empirical linear model between GPP_EC and SIF during the growing season (Fig. 1). This GPP-SIF relationship was used to estimate GPP (GPP_SIF) for the USNe1 site. The predicted GPP (GPP_SIF) for the USNe1 site was evaluated against GPP_EC. For comparison, we also estimated GPP using VPM and SCOPE models (GPP_VPM and GPP_SCOPE, respectively) for the USNe1 site.

Percentage of maize cropland within a MODIS pixel (500 m) and a 0.5 × 0.5 degree grid

To show the changes in proportion of croplands (maize and soybean) for the MODIS and GOME-2 grid pixels that cover the flux tower, we used the United States Department of Agriculture Cropland Data Layer (CDL) dataset for the study period (2007–2011) and aggregated 60-m data into 500-m and 0.5× 0.5 degree grid cells, respectively. Within the MODIS and GOME-2 grid pixels, vegetation cover was dominated by maize and soybean (Table 1).

[7] http://ameriflux.lbl.gov/

[8] http://www.bgc-jena.mpg.de/~MDIwork/eddyproc/

TABLE 1. Changes in proportion of croplands within the grid cell of Moderate Resolution Imaging Spectroradiometer (MODIS, 500 × 500 m) and Global Ozone Monitoring Experiment-2 (GOME-2, 0.5° × 0.5°) containing the Mead flux towers during 2007–2011.

	MODIS pixel (%)			GOME-2 (%)		
Year	Maize	Soybean	Total cultivated	Maize	Soybean	Total cultivated
2007	90.91	0.00	90.91	36.04	28.36	65.68
2008	82.43	4.05	94.59	32.88	36.50	85.60
2009	90.91	0.00	92.42	37.24	31.41	85.30
2010	87.03	3.35	97.91	36.64	34.97	87.50
2011	48.95	43.04	97.89	40.30	32.83	87.67

MODIS data

The surface reflectance 8-d L3 Global 500-m product (MOD09A1) for the study sites were extracted from the data portal of the Earth Observation and Modeling Facility, the University of Oklahoma (*available online*) using the geo-location coordinate of each flux tower.[9] A pixel-based quality assurance (QA) control was applied to generate a less noisy time series dataset by removing the noise of low quality, cloud, and aerosol contaminated pixels (Xiao et al. 2005). Eight-day composite values of EVI (Huete et al. 2002) and LSWI (Xiao et al. 2004) were calculated. The MOD15A2 FPAR product, a standard 8-d $FAPAR_{canopy}$ product for EOS-MODIS (Myneni et al. 2002), and the standard MODIS GPP product (GPP_MODIS), just for the comparison with other GPP estimates, were downloaded from the Oak Ridge National Laboratory Distributed Active Archive Center (ORNL DAAC) website (*data available online*).[10] $APAR_{canopy}$ and $APAR_{chl}$ were calculated by multiplying $FPAR_{canopy}$ and $FPAR_{chl}$ (equivalent to EVI in this study) with PAR which was measured at the flux sites. To determine the start and end dates of the maize growing season, we chose a threshold of LSWI ≥ −0.1 and GPP_EC ≥ 1 g C·m^2·d for the study sites according to Kalfas et al. (2011). For SIF and EVI, we fitted Savitsky-Golay functions using TIMESAT software to estimate onset and end of the growing season (Jönsson and Eklundh 2004).

VPM and input parameters

VPM estimates GPP as

$$GPP_{VPM} = \varepsilon_g \times FPAR_{chl} \times PAR, \quad (3)$$

where ε_g is light-use efficiency (LUE, g C/mol photosynthetic photon flux density [PPFD]), $FPAR_{chl}$ is fraction of PAR absorbed by chlorophyll, and PAR is photosynthetically active radiation. VPM uses EVI as $FPAR_{chl}$. While the detailed description of VPM has been provided previously (Xiao et al. 2004, Wagle et al. 2014), we briefly summarize it here.

[9] http://eomf.ou.edu/visualization/

[10] http://daac.ornl.gov/MODIS/

The VPM employs down-regulating scalars (ranging from 0 to 1) to characterize the effects of temperature (T_{scalar}) and water stress (W_{scalar}) on the LUE (ε_g) as

$$\varepsilon_g = \varepsilon_0 \times T_{scalar} \times W_{scalar}, \quad (4)$$

where ε_0 is the apparent quantum yield or maximum light use efficiency (g C/mol PPFD). A theoretical ε_0 value of 1.5 g C/mol PPFD was used in this study, as reported in a previous study (Kalfas et al. 2011). T_{scalar} was calculated at each time step as in the terrestrial ecosystem model (Raich et al. 1991) as

$$T_{scalar} = \frac{(T - T_{min})(T - T_{max})}{[(T - T_{min})(T - T_{max})] - (T - T_{opt})^2}, \quad (5)$$

where T is the air temperature and T_{min}, T_{max}, and T_{opt} represent the minimum, maximum, and optimum temperatures for photosynthesis, respectively. T_{min}, T_{max}, and T_{opt} were set to 10°, 48°, and 28°C, respectively, as in Kalfas et al. (2011). LSWI was used to account for the effect of water stress on photosynthesis as

$$W_{scalar} = \frac{1 + LSWI}{1 + LSWI_{max}}, \quad (6)$$

where $LSWI_{max}$ is the maximum LSWI within the plant growing season.

SCOPE model and input parameters

The SCOPE model is a vertical (1D) biophysical model that couples radiative transfer of optical and thermal radiation with the leaf biochemical process (Van der Tol et al. 2009*a*). The biochemical components for C_3 and C_4 plants are based on Collatz et al. (1991, 1992). It simulates within-canopy vertical heat flux distribution, the hyperspectral outgoing radiances (Verhoef and Bach 2007), and the photosynthesis of C_3 or C_4 vegetation. It describes sun-canopy-observer geometry and leaf orientation to consider different biophysical processes for sunlit and shaded components. The novelty of SCOPE is that it couples a leaf-level chlorophyll fluorescence model (Van der Tol et al. 2009*b*) with a leaf biochemical model to calculate top-of-canopy chlorophyll fluorescence. Radiative transfer of chlorophyll fluorescence is

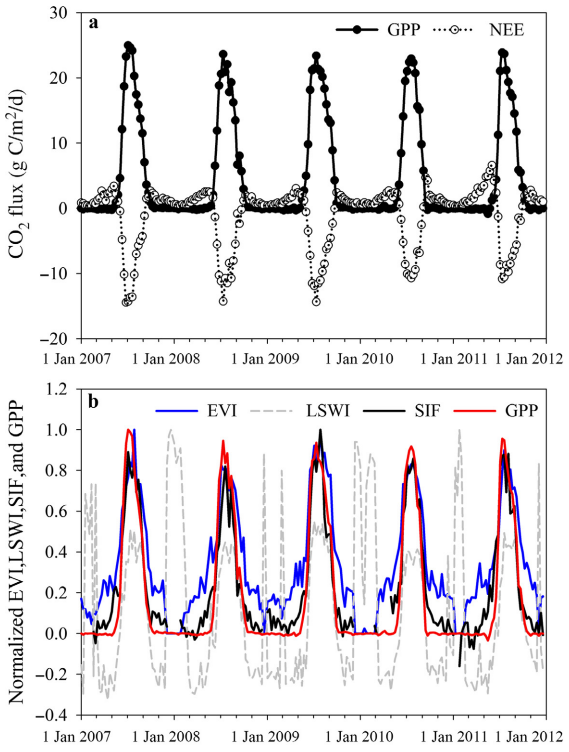

FIG. 2. Seasonal dynamics of (a) net ecosystem CO_2 exchange (NEE) and gross primary production (GPP), and (b) enhanced vegetation index (EVI), land surface water index (LSWI), sun-induced chlorophyll inflorescence (SIF), and GPP at the USNe1 site during 2007–2011.

calculated using a module similar to the FluorSAIL model (Miller et al. 2005), but one that allows leaf fluorescence to vary depending on position and orientation in the canopy. A leaf-level biochemical model calculates 400–700 nm range fluorescence from the absorbed fluxes, canopy temperature, and ambient vapor, and CO_2 and O_2 concentrations in conjunction with GPP, stomatal resistance, and the energy balance of the leaf (Van der Tol et al. 2009b). The model calculates radiative transfer in a multilayer canopy as a function of the solar zenith angle and leaf orientation to simulate fluorescence in the observation direction. More details of this model can be found in Van der Tol et al. (2009*a*). We used a recent version of SCOPE (v1.52) in this study.

Running SCOPE for photosynthesis and fluorescence requires inputs of meteorological forcing (incoming shortwave and long-wave radiation, air temperature and pressure, humidity, wind speed, and CO_2 concentration), LAI, leaf angle distribution, leaf chlorophyll content (C_{ab}), stomatal conductance parameter (m), and maximum carboxylation capacity (V_{cmax}). Meteorological inputs and LAI for SCOPE were available from the site measurements. Leaf angle distribution was assumed to be spherical, which is a good approximation in crops such as maize (Verhoef and Bach 2007). An estimation of C_{ab} controlling the leaf and canopy radiative transfer was

TABLE 2. Start, peak, and end dates of maize growing season during 2007–2011 at the USNe1 site based on tower-based gross primary production (GPP_EC), land surface water index (LSWI), enhanced vegetation index (EVI), and sun-induced chlorophyll inflorescence (SIF).

	GPP > 1 (g C/m^2/d)			LSWI > −0.1			EVI			SIF		
Year	Start	Peak	End	Start	Peak	End	Start	Peak	End	Start	Peak	End
2007	25 May	19 Jul	22 Sep	25 May	5 Aug	30 Sep	5 May	1 Aug	28 Nov	19 May	25 Jul	21 Sep
2008	1 Jun	27 Jul	7 Oct	24 May	13 Aug	29 Sep	16 Mar	31 Jul	25 Oct	25 May	1 Aug	5 Oct
2009	17 May	25 Jul	22 Sep	10 Jun	5 Aug	8 Oct	2 May	3 Aug	3 Dec	31 May	25 Jul	5 Oct
2010	25 May	26 Jul	6 Sep	25 May	2 Aug	14 Sep	21 Mar	7 Jul	13 Dec	28 May	29 Jul	28 Sep
2011	2 Jun	29 Jul	8 Oct	10 Jun	19 Aug	24 Oct	30 Mar	9 Aug	7 Nov	27 May	2 Aug	29 Sep

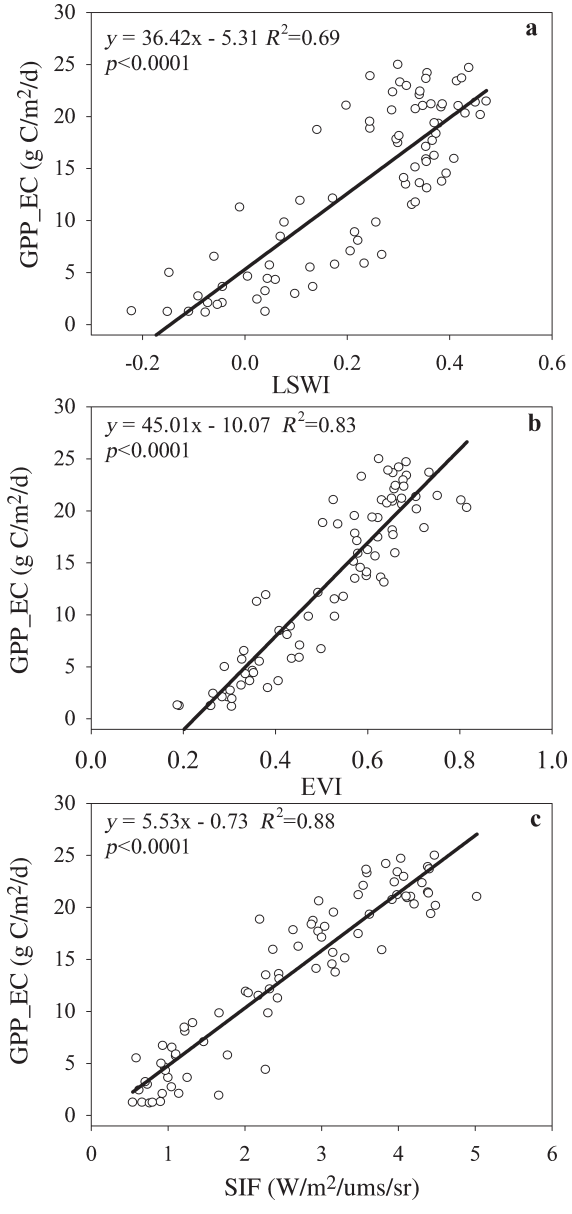

FIG. 3. Relationships between tower-based gross primary production (GPP_EC) and (a) land surface water index (LSWI), (b) enhanced vegetation index (EVI), and (c) sun-induced chlorophyll inflorescence (SIF) for the USNe1 site during the 2007–2011 growing season.

inverted from vegetation indices (EVI and MERIS terrestrial chlorophyll index, MTCI (Dash and Curran 2004)), and seasonal V_{cmax} was inverted from GOME-2 SIF measurements as described in Zhang et al. (2014). The SCOPE model was constrained by optimizing the key parameter of V_{cmax} by combining with GOME-SIF data, as discussed in Zhang et al. (2014). The SCOPE was first run in forward mode, and a link between canopy SIF and V_{cmax} was derived as a look-up table. Then, SIF retrievals from GOME-2 were used to derive V_{cmax} for the crop flux site. The optimized V_{cmax} values are seasonally varied, characterized with peak in the mid-growing season (see Fig. 4 in Zhang et al. 2014). Other parameters of the SCOPE model, such as reflectance and transmittance of vegetation and soil, were set to default values.

RESULTS

Consistency of maize phenology observed by seasonal dynamics of GPP, LSWI, EVI, and SIF

To examine the consistency of maize phenology, seasonal dynamics of NEE, GPP, LSWI, EVI, and SIF from 2007 to 2011 at the USNe1 site is presented in Fig. 2. Crop photosynthesis started around late May or early June with a rapid rise in NEE and GPP and ended in late September with NEE and GPP approaching zero (Fig. 2a). Both LSWI and SIF started to increase in late May to early June, indicating the beginning of the growing season (Fig. 2b, Table 2). SIF peaked in late July and declined to low values by late September to early October, which is consistent with the trends of GPP and NEE. LSWI peaked around two weeks later than GPP and SIF (Table 2). EVI shows consistently earlier onset and later senescence of maize (Fig. 2b and Table 2). We also noted that EVI was generally above 0.1 in the spring and autumn due to the effects of soil and snow when

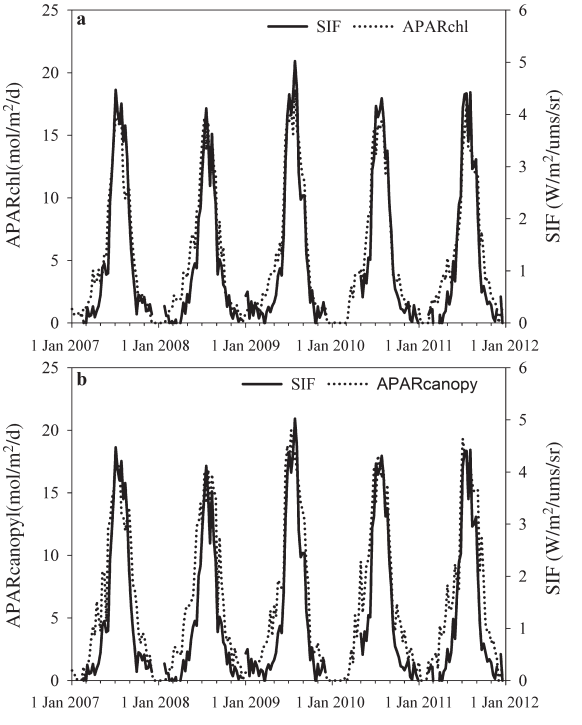

FIG. 4. Seasonal dynamics of absorbed photosynthetically active radiation by canopy ($APAR_{canopy}$) and chlorophyll ($APAR_{chl}$), and sun-induced chlorophyll inflorescence (SIF) at the USNe1 site during 2007–2011.

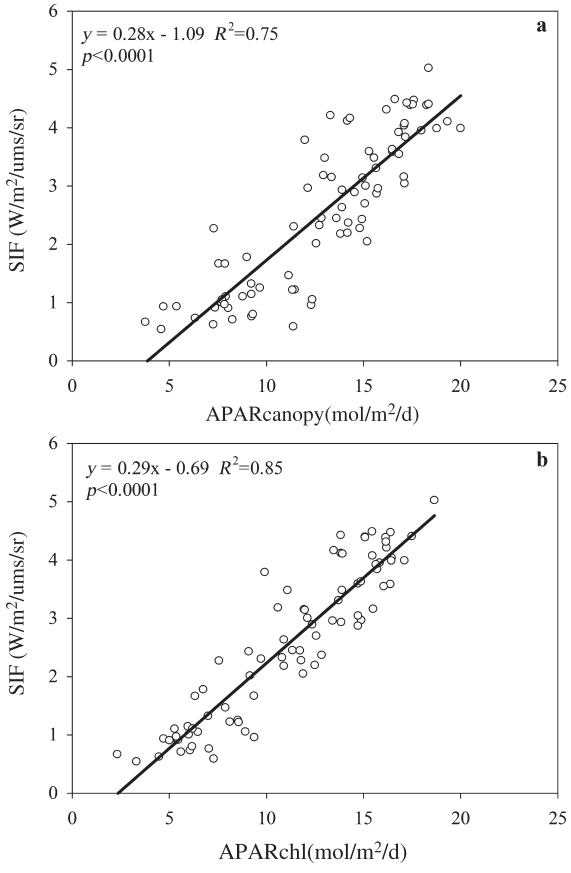

FIG. 5. Relationships between 8-d sun-induced chlorophyll inflorescence (SIF) and absorbed photosynthetically active radiation by (a) canopy ($APAR_{canopy}$) and (b) chlorophyll ($APAR_{chl}$) at the USNe1 site during the 2007–2011 growing season.

there was no photosynthetic activity, while SIF values were approximately zero (Fig. 2b). These results illustrate that SIF was much better at capturing seasonal variations (particularly during early and late season) in GPP compared with remotely sensed vegetation indices (LSWI and EVI). As a result, SIF showed a stronger linear relationship with GPP_EC (R^2 = 0.88) than did LSWI (R^2 = 0.69) and EVI (R^2 = 0.83) when relationships of GPP_EC with SIF, EVI, and LSWI were compared during the growing season at the USNe1 site (Fig. 3).

Seasonal dynamics of $APAR_{canopy}$ and $APAR_{chl}$ were compared with the seasonal dynamics of SIF during 2007–2011 in Fig. 4. The $APAR_{chl}$ was generally lower than the $APAR_{canopy}$. Overall, SIF tracked seasonal dynamics of both $APAR_{canopy}$ and $APAR_{chl}$ well. However, $APAR_{canopy}$ showed earlier springtime rise and later autumn decline and also a slightly longer growing season across years when compared with SIF (Fig. 4b), while $APAR_{chl}$ time series showed more consistent seasonality with SIF (Fig. 4a). Consequently, a stronger linear relationship was found between $APAR_{chl}$ and SIF (R^2 = 0.92 and RMSE=0.51) than between $APAR_{canopy}$ and SIF (R^2 = 0.86 and RMSE=0.65; Fig. 5). The results indicate that SIF is more related to photosynthetic components of chlorophyll-containing foliage in the canopy (here $FPAR_{chl}$) than the entire canopy (here $FPAR_{canopy}$, MOD15A2 FPAR), which is composed of both photosynthetic (mostly green leaves) and non-photosynthetic (mostly senescent foliage and stems) parts of vegetation.

Comparison of GPP predicted by VPM, SCOPE, and SIF models

Comparison of seasonal dynamics of GPP_EC, GPP_VPM, GPP_SCOPE, GPP_SIF, and GPP_MODIS during the 2007–2011 growing season at the USNe1 site shows that GPP_VPM, GPP_SCOPE, and GPP_SIF tracked the magnitude and seasonal dynamics of GPP_EC well (Fig. 6). This is also supported by strong positive relationships (R^2 = 0.87–0.95) of GPP_EC with GPP_VPM, GPP_SCOPE, and GPP_SIF (Fig. 7). However, GPP_MODIS was substantially lower compared to other GPP estimates and GPP_EC and showed a poor correlation with GPP_EC (R^2 = 0.47). These results illustrated good performance of all three approaches, which were significantly improved compared to the standard MOD17 GPP algorithm in estimating maize GPP. Among those three approaches, SCOPE and SIF slightly underestimated maize GPP, while VPM slightly overestimated it when they were compared to GPP_EC. Our results show that SCOPE model showed the best performance (RMSE = 1.58 g C/m^2/d and R^2 = 0.95) than did VPM (RMSE = 2.27 g C/m^2/d and R^2 = 0.91) and SIF (RMSE = 2.72 g C/m^2/d and R^2 = 0.87). Seasonal sums of GPP_EC, GPP_VPM, GPP_SCOPE, and GPP_SIF over the growing season for the USNe1 site are provided in Table 3. On an average, the percentage of relative error (% RE) ranged from 6.3% for VPM to −4.3% for SCOPE and −5.5% for SIF during 2007–2011. For SCOPE and SIF approaches, GPP estimations were especially low in 2008 (−12.4% and

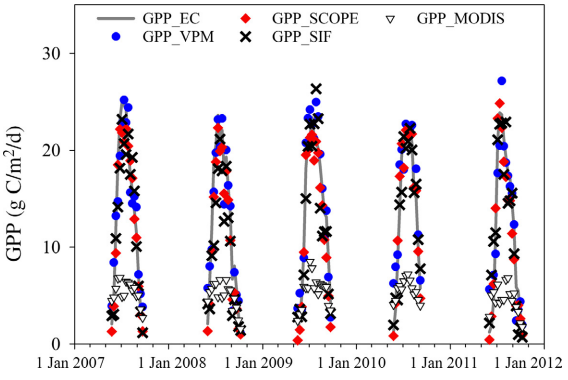

FIG. 6. Seasonal dynamics of tower-based gross primary production (GPP_EC) and predicted GPP by VPM (GPP_VPM), SCOPE (GPP_SCOPE), SIF (GPP_SIF), and the standard MOD17 GPP product (GPP_MODIS) during the 2007–2011 growing season at the USNe1 site.

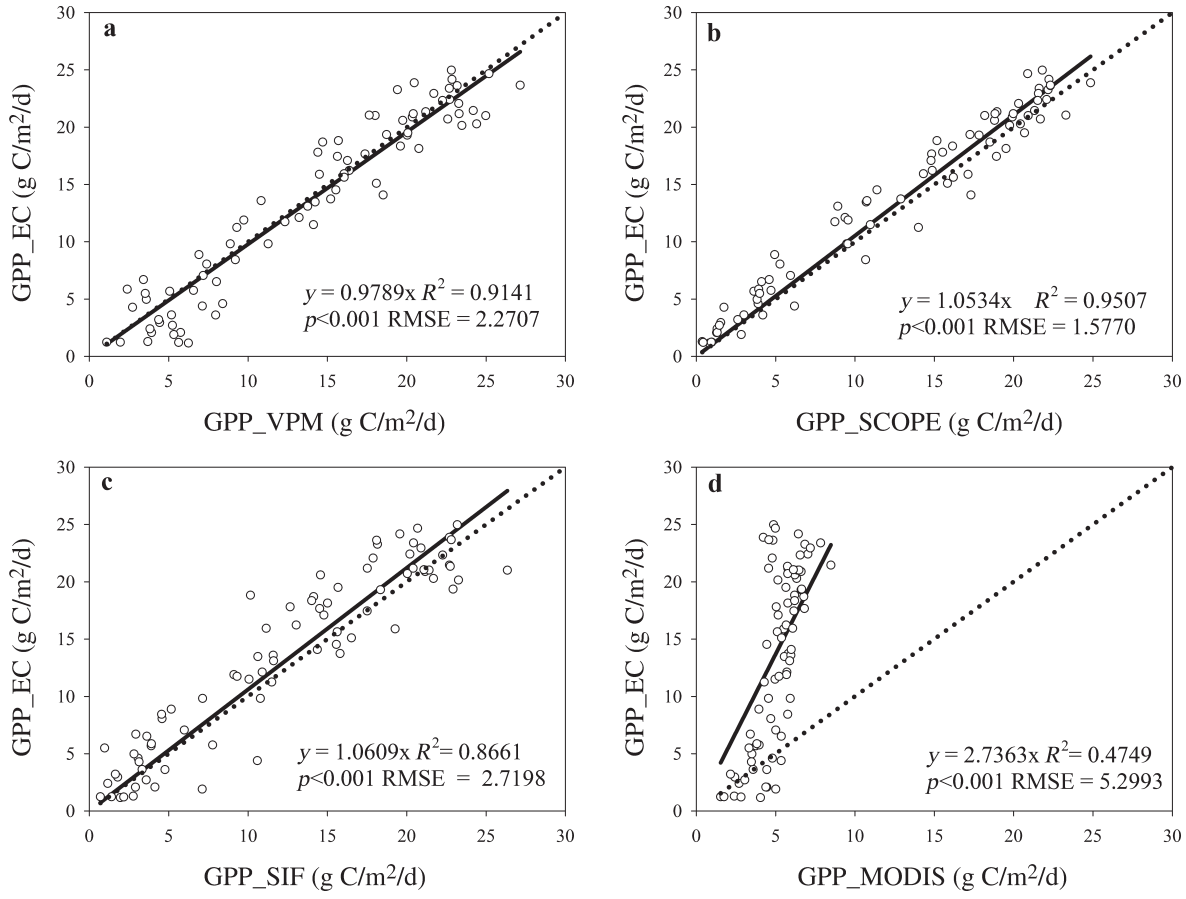

FIG. 7. Relationships between tower-based gross primary production (GPP_EC) and predicted GPP by (a) VPM (GPP_VPM), (b) SCOPE (GPP_SCOPE), (c) SIF (GPP_SIF), and (d) the standard MOD17 GPP product (GPP_MODIS) for the USNe1 site during the 2007–2011 growing season.

TABLE 3. Annual sums of tower-based gross primary production (GPP_EC) and predicted GPP by VPM (GPP_VPM), SCOPE (GPP_SCOPE), and sun-induced chlorophyll inflorescence (GPP_SIF) at the USNe1 site during the maize growing season.

Year	GPP_EC	GPP_VPM	RE	GPP_SCOPE	RE	GPP_SIF	RE
2007	1754.3	1844.2	5.1	1685.9	−3.9	1659.1	−5.4
2008	1703.7	1697.4	−0.4	1491.7	−12.4	1343.8	−21.1
2009	1840.0	2014.6	9.5	1711.9	−7.0	1790.6	−2.7
2010	1566.0	1769.7	13.0	1640.1	4.7	1574.3	0.5
2011	1578.1	1643.8	4.2	1530.0	−3.0	1598.0	1.3

Notes: Unit is in g C/m^2. RE (%) is relative error of GPP_VPM, GPP_SCOPE, and GPP_SIF compared to GPP_EC.

−21.1%, respectively), while VPM overestimated GPP estimates by 13% in 2010.

DISCUSSION

Vegetation indices have often been used to identify crop phenology for cropland management and productivity estimation (Churkina et al. 2005, Fisher et al. 2006, Jans et al. 2010, Wagle et al. 2015). Recently, space-borne SIF observations have provided an alternative way to monitor photosynthesis from space (Frankenberg et al. 2011, Guanter et al. 2014). In this current study, the comparison of vegetation indices, including EVI and LSWI, and SIF with tower-based CO_2 flux showed the consistency of SIF in characterizing the start and end dates of the maize growing season at the USNe1 site (Fig. 2 and Table 2). It was also found that SIF showed a stronger relationship with GPP_EC (R^2 = 0.88) than did EVI (R^2 = 0.83) and LSWI (R^2 = 0.69; Fig. 3). Results show that EVI performed poorly in describing maize

phenology (Fig. 2b), consistent with the finding of a previous study (Richardson et al. 2012). SIF also showed a slightly earlier onset of the growing season as compared with the GPP_EC (Fig. 2b). This can be attributed to the spatial differences of GOME-2 footprint and flux tower footprint. The larger footprints of GOME-2 SIF probably contained more than one crop and other vegetation types. However, considering the fact that GOME-2 sensors are not yet optimized for SIF measurements, our results demonstrate that space-borne SIF can provide an additional way to investigate the seasonality of photosynthetic activity of maize.

The comparison of SIF with $APAR_{canopy}$ and $APAR_{chl}$ suggested that SIF is more related to PAR absorbed by photosynthetic components of maize canopy (Figs. 4 and 5). Assuming a constant LUE in canopy photosynthesis for crops in Eq. 2 (Ruimy et al. 1996), variations of canopy chlorophyll fluorescence are dependent on $APAR_{chl}$ for maize. Hence, though SIF measured from space is the amount of photons that are re-emitted from the whole canopy, Figs. 4 and 5 suggest that SIF is more driven by photosynthetic components of canopy because only the PAR absorbed by photosynthetic pigments ($APAR_{chl}$) drives leaf photosynthesis and chlorophyll fluorescence. The PAR absorbed by non-photosynthetic components (e. g., senescent foliage, branches, stems, and litter) cannot be used in carbon assimilation and chlorophyll fluorescence generation processes. The MOD15A2 FPAR product utilizes reflectance from the whole vegetation canopy, including the influence of non-photosynthetic components (Zhang et al. 2005, 2009), resulting in slightly overestimation of the actual APAR (Fig. 4) and weaker relationship between $FPAR_{canopy}$ and SIF than between $FPAR_{chl}$ and SIF (Fig. 5). It should be noted that, as in this study, EVI has been used to estimate or replace $FPAR_{chl}$ in several studies (Xiao et al. 2004, Gitelson et al. 2006, Sims et al. 2008). Recently, it has been shown that other vegetation indices such as MTCI had a slightly stronger linear relationship with $FPAR_{chl}$ than did EVI and NDVI due to its accurate representation of canopy chlorophyll content (Ogutu and Dash 2013). More direct retrieval of $FPAR_{chl}$ has emerged from MODIS reflectance data and a radiative transfer model (Zhang et al. 2005, 2009), showing more consistent results with CO_2 flux for cropland and broadleaf forest sites (Cheng et al. 2014). These improved products can be used for further analysis in the future.

The performance of the three GPP modeling approaches (VPM, SCOPE, and SIF) was highly consistent in their predictions of seasonal dynamics and magnitudes of GPP as compared with GPP_EC (Fig. 6). Consequently, there were strong positive relationships between predicted GPPs and GPP_EC (Fig. 7) and discrepancies of the seasonal sums of predicted GPPs and GPP_EC were small ($RE < \pm 10\%$ in most cases; Table 3). The underestimation for SCOPE and SIF approaches in 2008 was due to the lower SIF value in 2008 because the persisted wet and cool weather in spring 2008 (the Midwest flood) had delayed maize planting in this area (Hatfield 2012). However, maize was still planted on schedule (April 29) at the Mead site (USNe1). Because of the spatial mismatch between GOME-2 and flux tower footprints, SIF might not reflect the flux tower conditions well in this condition. Among three approaches, the process-based SCOPE model showed the best performance by constraining the V_{cmax} parameter derived from satellite retrievals of SIF. Space-borne SIF observations can be used to retrieve the seasonal variability of V_{cmax} for maize and soybean (Zhang et al. 2014). Their results showed that incorporation of seasonally varying V_{cmax} through SIF improved the modeling of GPP and LUE for both C_3 and C_4 crops compared to an invariant V_{cmax} used in the SCOPE model. The consistency of GPP estimates by SCOPE and other two approaches in this study highlights the use of SIF for the benchmarking of process-based TMBs. Our results illustrate that space-borne SIF can be used not only to constrain process-based models for improving GPP predictions but also to develop an empirical relationship with GPP_EC (as shown in Fig. 1) to accurately estimate and extrapolate GPP over large maize cropland areas.

Our results show that the standard MOD17 GPP product significantly underestimated GPP for this high productive maize site (Fig. 6), consistent with the findings of previous studies in croplands (Chen et al. 2011, Guanter et al. 2014, Zhang et al. 2014, Wagle et al. 2015). The main reason for such significant underestimation is that the MOD17 GPP algorithm assumes only one crop type in the biome properties look-up table (BPLUT; Running et al. 2004) and uses a maximum crop LUE of 0.30 g C/mol PPFD for both C_3 and C_4 crops, which is substantially smaller than the values for both maize (C_4 type) and soybean (C_3 type; Cheng et al. 2014, Zhang et al. 2014, Wagle et al. 2015). Hence, even though the MOD17 GPP algorithm utilizes an overestimation of in-situ FPAR from the MODIS FPAR product ($FPAR_{canopy}$), it is not enough to offset too low prescribed maximum LUE (Heinsch et al. 2006, Wagle et al. 2014), which leads to underestimation of GPP.

Conclusions

Considering large uncertainties associated with current GPP models, especially for croplands (Huntzinger et al. 2012, Schaefer et al. 2012), there is a pressing need for additional data to constrain the GPP model estimates. In this study, we evaluated the ability of three different approaches (LUE-based VPM, process-based SCOPE, and space-borne SIF) to estimate GPP at a maize site in Mead, Nebraska, USA. Overall, all three approaches captured seasonal dynamics and magnitude of maize GPP well as compared with GPP_EC, and they were significantly improved compared to the MOD17 GPP product. Our results illustrate that, by integrating with GPP_EC, space-borne SIF can provide reasonable estimates of maize GPP without using additional

information such as climate inputs and satellite-based vegetation indices which are required by the process-based (SCOPE) and satellite-based LUE (VPM) models, and data-oriented diagnostic techniques based on the FLUXNET network of tower sites and remote sensing vegetation indices (Jung et al. 2011). Furthermore, space-borne SIF data not only can provide an additional way to investigate the seasonality of photosynthetic activity of maize, but also can constrain process-based GPP models for improving GPP estimates. It should be noted that the assumption of homogenous landscape within the footprint of GOME-2 is tenuous and we acknowledge the inherent difficulties to compare it with relatively small spatial scale of flux tower measurements. With the launch of the Orbiting Carbon Observatory-2 (OCO-2) (Frankenberg et al. 2014) in 2014 and the Sentinel-5 Precursor (TROPOMI; Veefkind et al. 2012) satellite missions in 2016, availability of a higher spatial resolution more space-borne SIF data would be more helpful to address this issue. In addition, whether our evaluations hold beyond the maize considered in this study is a question for future research to address, and an additional work is needed to expand this analysis to other crop types such as C_3 crops (soybean and wheat) for a cross-site comparison.

Acknowledgments

This work was supported by the Thousand Young Talents Program in China and the National Science Foundation of China (#41371070) to Y. Zhang, and the USDA National Institute for Food and Agriculture (#2013-69002) and the National Science Foundation (IIA-1301789) to P. Wagle, X. Xiao, and C. Jin. We thank Dr. Andrew Suyker (University of Nebraska) for the Mead flux tower data. We would also like to thank Sarah L. Xiao at Yale University for the English correction. We are grateful to two anonymous reviewers for constructing suggestions which helped us improve the manuscript.

Literature Cited

Chen, T., G. R. van der Werf, A. Dolman, and M. Groenendijk. 2011. Evaluation of cropland maximum light use efficiency using eddy flux measurements in North America and Europe. Geophysical Research Letters 38, L14707, doi:10.1029/2011GL047533.

Cheng, Y.-B., Q. Zhang, A. I. Lyapustin, Y. Wang, and E. M. Middleton. 2014. Impacts of light use efficiency and fPAR parameterization on gross primary production modeling. Agricultural and Forest Meteorology 189:187–197.

Churkina, G., D. Schimel, B. H. Braswell, and X. Xiao. 2005. Spatial analysis of growing season length control over net ecosystem exchange. Global Change Biology 11:1777–1787.

Collatz, G. J., J. T. Ball, C. Grivet, and J. A. Berry. 1991. Physiological and environmental regulation of stomatal conductance, photosynthesis and transpiration: a model that includes a laminar boundary layer. Agricultural and Forest Meteorology 54:107–136.

Collatz, G. J., M. Ribas-Carbo, and J. Berry. 1992. Coupled photosynthesis-stomatal conductance model for leaves of C_4 plants. Functional Plant Biology 19:519–538.

Dash, J., and P. Curran. 2004. The MERIS terrestrial chlorophyll index. International Journal of Remote Sensing, 25:5403-5413.

FAO. 2013. Statistical yearbook 2013: world food and agriculture. Food and Agriculture Organization of the United Nations, Rome.

Farquhar, G. D., S. von Caemmerer, and J. A. Berry. 1980. A biochemical model of photosynthetic CO_2 assimilation in leaves of C_3 species. Planta 149:78–90.

Fisher, J. I., J. F. Mustard, and M. A. Vadeboncoeur. 2006. Green leaf phenology at Landsat resolution: scaling from the field to the satellite. Remote Sensing of Environment 100:265–279.

Frankenberg, C., J. B. Fisher, J. Worden, G. Badgley, S. S. Saatchi, J. E. Lee, G. C. Toon, A. Butz, M. Jung, and A. Kuze. 2011. New global observations of the terrestrial carbon cycle from GOSAT: patterns of plant fluorescence with gross primary productivity. Geophysical Research Letters 38, L17706, doi:10.1029/2011GL048738.

Frankenberg, C., C. O'Dell, J. Berry, L. Guanter, J. Joiner, P. Köhler, R. Pollock, and T. E. Taylor. 2014. Prospects for chlorophyll fluorescence remote sensing from the Orbiting Carbon Observatory-2. Remote Sensing of Environment 147:1–12.

Friedl, M. A., D. Sulla-Menashe, B. Tan, A. Schneider, N. Ramankutty, A. Sibley, and X. Huang. 2010. MODIS Collection 5 global land cover: algorithm refinements and characterization of new datasets. Remote Sensing of Environment 114:168–182.

Gitelson, A. A., A. Viña, S. B. Verma, D. C. Rundquist, T. J. Arkebauer, G. Keydan, B. Leavitt, V. Ciganda, G. G. Burba, and A. E. Suyker. 2006. Relationship between gross primary production and chlorophyll content in crops: implications for the synoptic monitoring of vegetation productivity. Journal of Geophysical Research: Atmospheres 111:D08S11.

Gray, J. M., S. Frolking, E. A. Kort, D. K. Ray, C. J. Kucharik, N. Ramankutty, and M. A. Friedl. 2014. Direct human influence on atmospheric CO_2 seasonality from increased cropland productivity. Nature 515:398–401.

Guanter, L., C. Frankenberg, A. Dudhia, P. E. Lewis, J. Gómez-Dans, A. Kuze, H. Suto, and R. G. Grainger. 2012. Retrieval and global assessment of terrestrial chlorophyll fluorescence from GOSAT space measurements. Remote Sensing of Environment 121:236–251.

Guanter, L., Y. Zhang, M. Jung, J. Joiner, M. Voigt, J. A. Berry, C. Frankenberg, A. R. Huete, P. Zarco-Tejada, and J.-E. Lee. 2014. Global and time-resolved monitoring of crop photosynthesis with chlorophyll fluorescence. Proceedings of the National Academy of Sciences USA 111:E1327–E1333.

Hatfield, J., 2012. Agriculture in the Midwest. In: US National Climate Assessment Midwest Technical Input Report. J. Winkler, J. Andresen, J. Hatfield, D. Bidwell, and D. Brown, coordinators. Available from the Great Lakes Integrated Sciences and Assessments (GLISA) Center, http://glisa.msu.edu/docs/NCA/MTIT_Agriculture.pdf.

Heinsch, F. A., M. Zhao, S. W. Running, J. S. Kimball, R. R. Nemani, K. J. Davis, P. V. Bolstad, B. D. Cook, A. R. Desai, and D. M. Ricciuto. 2006. Evaluation of remote sensing based terrestrial productivity from MODIS using regional tower eddy flux network observations. IEEE Transactions on Geoscience and Remote Sensing 44: 1908–1925.

Hilker, T., N. C. Coops, M. A. Wulder, T. A. Black, and R. D. Guy. 2008. The use of remote sensing in light use efficiency based models of gross primary production: a

review of current status and future requirements. Science of the Total Environment 404:411–423.

Huete, A., K. Didan, T. Miura, E. P. Rodriguez, X. Gao, and L. G. Ferreira. 2002. Overview of the radiometric and biophysical performance of the MODIS vegetation indices. Remote Sensing of Environment 83:195–213.

Huntzinger, D., W. M. Post, Y. Wei, A. Michalak, T. O. West, A. Jacobson, I. Baker, J. M. Chen, K. Davis, and D. Hayes. 2012. North American Carbon Program (NACP) regional interim synthesis: terrestrial biospheric model intercomparison. Ecological Modelling 232:144–157.

Jans, W. W., C. M. Jacobs, B. Kruijt, J. A. Elbers, S. Barendse, and E. J. Moors. 2010. Carbon exchange of a maize (*Zea mays* L.) crop: influence of phenology. Agriculture, Ecosystems & Environment 139:316–324.

Jin, C., X. Xiao, P. Wagle, T. Griffis, J. Dong, C. Wu, Y. Qin, and D. R. Cook. 2015. Effects of in-situ and reanalysis climate data on estimation of cropland gross primary production using the vegetation photosynthesis model. Agricultural and Forest Meteorology 213:240–250.

Joiner, J., Y. Yoshida, A. Vasilkov, and E. Middleton. 2011. First observations of global and seasonal terrestrial chlorophyll fluorescence from space. Biogeosciences 8:637–651.

Joiner, J., L. Guanter, R. Lindstrot, M. Voigt, A. Vasilkov, E. Middleton, K. Huemmrich, Y. Yoshida, and C. Frankenberg. 2013. Global monitoring of terrestrial chlorophyll fluorescence from moderate-spectral-resolution near-infrared satellite measurements: methodology, simulations, and application to GOME-2. Atmospheric Measurement Techniques 6:2803–2823.

Joiner, J., Y. Yoshida, A. Vasilkov, K. Schaefer, M. Jung, L. Guanter, Y. Zhang, S. Garrity, E. Middleton, and K. Huemmrich. 2014. The seasonal cycle of satellite chlorophyll fluorescence observations and its relationship to vegetation phenology and ecosystem atmosphere carbon exchange. Remote Sensing of Environment 152:375–391.

Jönsson, P., and L. Eklundh. 2004. TIMESAT: a program for analyzing time-series of satellite sensor data. Computers & Geosciences 30:833–845.

Jung, M., M. Vetter, M. Herold, G. Churkina, M. Reichstein, S. Zaehle, P. Ciais, N. Viovy, A. Bondeau, and Y. Chen. 2007. Uncertainties of modeling gross primary productivity over Europe: a systematic study on the effects of using different drivers and terrestrial biosphere models. Global Biogeochemical Cycles 21, GB4021, doi:10.1029/2006GB 002915.

Jung, M., M. Reichstein, H. A. Margolis, A. Cescatti, A. D. Richardson, M. A. Arain, A. Arneth, C. Bernhofer, D. Bonal, and J. Chen. 2011. Global patterns of land-atmosphere fluxes of carbon dioxide, latent heat, and sensible heat derived from eddy covariance, satellite, and meteorological observations. Journal of Geophysical Research: Biogeosciences 2005–2012:116.

Kalfas, J. L., X. Xiao, D. X. Vanegas, S. B. Verma, and A. E. Suyker. 2011. Modeling gross primary production of irrigated and rain-fed maize using MODIS imagery and CO_2 flux tower data. Agricultural and Forest Meteorology 151:1514–1528.

Miller, J., M. Berger, Y. Goulas, S. Jacquemoud, J. Louis, G. Mohammed, N. Moise, J. Moreno, I. Moya, and R. Pedrós. 2005. Development of a vegetation fluorescence canopy model. ESTEC Contract 16365.

Monteith, J. 1972. Solar radiation and productivity in tropical ecosystems. Journal of Applied Ecology 9:747–766.

Myneni, R., S. Hoffman, Y. Knyazikhin, J. Privette, J. Glassy, Y. Tian, Y. Wang, X. Song, Y. Zhang, and G. Smith. 2002. Global products of vegetation leaf area and fraction absorbed PAR from year one of MODIS data. Remote Sensing of Environment 83:214–231.

Nightingale, J., N. Coops, R. Waring, and W. Hargrove. 2007. Comparison of MODIS gross primary production estimates for forests across the USA with those generated by a simple process model, 3-PGS. Remote Sensing of Environment 109:500–509.

Ogutu, B. O., and J. Dash. 2013. An algorithm to derive the fraction of photosynthetically active radiation absorbed by photosynthetic elements of the canopy (FAPARps) from eddy covariance flux tower data. New Phytologist 197:511–523.

Peters, W., A. R. Jacobson, C. Sweeney, A. E. Andrews, T. J. Conway, K. Masarie, J. B. Miller, L. M. Bruhwiler, G. Petron, and A. I. Hirsch. 2007. An atmospheric perspective on North American carbon dioxide exchange: CarbonTracker. Proceedings of the National Academy of Sciences 104:18925–18930.

Potter, C. S., J. T. Randerson, C. B. Field, P. A. Matson, P. M. Vitousek, H. A. Mooney, and S. A. Klooster. 1993. Terrestrial ecosystem production: a process model based on global satellite and surface data. Global Biogeochemical Cycles 7:811–841.

Raich, J., E. Rastetter, J. Melillo, D. Kicklighter, P. Steudler, B. Peterson, A. Grace, B. Moore Iii, and C. Vorosmarty. 1991. Potential net primary productivity in South America: application of a global model. Ecological Applications 1:399–429.

Reichstein, M., E. Falge, D. Baldocchi, D. Papale, M. Aubinet, P. Berbigier, C. Bernhofer, N. Buchmann, T. Gilmanov, and A. Granier. 2005. On the separation of net ecosystem exchange into assimilation and ecosystem respiration: review and improved algorithm. Global Change Biology 11:1424–1439.

Richardson, A. D., R. S. Anderson, M. A. Arain, A. G. Barr, G. Bohrer, G. Chen, J. M. Chen, P. Ciais, K. J. Davis, and A. R. Desai. 2012. Terrestrial biosphere models need better representation of vegetation phenology: results from the North American Carbon Program Site Synthesis. Global Change Biology 18:566–584.

Ruimy, A., G. Dedieu, and B. Saugier. 1996. TURC: a diagnostic model of continental gross primary productivity and net primary productivity. Global Biogeochemical Cycles 10:269–285.

Running, S. W., R. R. Nemani, F. A. Heinsch, M. Zhao, M. Reeves, and H. Hashimoto. 2004. A continuous satellite-derived measure of global terrestrial primary production. BioScience 54:547–560.

Schaefer, K., C. R. Schwalm, C. Williams, M. A. Arain, A. Barr, J. M. Chen, K. J. Davis, D. Dimitrov, T. W. Hilton, and D. Y. Hollinger. 2012. A model-data comparison of gross primary productivity: results from the North American Carbon Program site synthesis. Journal of Geophysical Research: Biogeosciences 2005–2012:117.

Sellers, P., R. Dickinson, D. Randall, A. Betts, F. Hall, J. Berry, G. Collatz, A. Denning, H. Mooney, and C. Nobre. 1997. Modeling the exchanges of energy, water, and carbon between continents and the atmosphere. Science 275:502–509.

Sims, D. A., A. F. Rahman, V. D. Cordova, B. Z. El-Masri, D. D. Baldocchi, P. V. Bolstad, L. B. Flanagan, A. H. Goldstein, D. Y. Hollinger, and L. Misson. 2008. A new model of gross primary productivity for North American ecosystems based solely on the enhanced vegetation index and land surface temperature from MODIS. Remote Sensing of Environment 112:1633–1646.

Suyker, A. E., and S. B. Verma. 2012. Gross primary production and ecosystem respiration of irrigated and rainfed maize–soybean cropping systems over 8 years. Agricultural and Forest Meteorology 165:12–24.

Van der Tol, C., W. Verhoef, J. Timmermans, A. Verhoef, and Z. Su. 2009a. An integrated model of soil-canopy spectral radiances, photosynthesis, fluorescence, temperature and energy balance. Biogeosciences 6:3109–3129.

Van der Tol, C., W. Verhoef, and A. Rosema. 2009b. A model for chlorophyll fluorescence and photosynthesis at leaf scale. Agricultural and Forest Meteorology 149:96–105.

Veefkind, J., I. Aben, K. McMullan, H. Förster, J. De Vries, G. Otter, J. Claas, H. Eskes, J. De Haan, and Q. Kleipool. 2012. TROPOMI on the ESA Sentinel-5 Precursor: a GMES mission for global observations of the atmospheric composition for climate, air quality and ozone layer applications. Remote Sensing of Environment 120:70–83.

Verhoef, W., and H. Bach. 2007. Coupled soil–leaf-canopy and atmosphere radiative transfer modeling to simulate hyperspectral multi-angular surface reflectance and TOA radiance data. Remote Sensing of Environment 109:166–182.

Verma, S. B., A. Dobermann, K. G. Cassman, D. T. Walters, J. M. Knops, T. J. Arkebauer, A. E. Suyker, G. G. Burba, B. Amos, and H. Yang. 2005. Annual carbon dioxide exchange in irrigated and rainfed maize-based agroecosystems. Agricultural and Forest Meteorology 131:77–96.

Wagle, P., X. Xiao, M. S. Torn, D. R. Cook, R. Matamala, M. L. Fischer, C. Jin, J. Dong, and C. Biradar. 2014. Sensitivity of vegetation indices and gross primary production of tallgrass prairie to severe drought. Remote Sensing of Environment 152:1–14.

Wagle, P., X. Xiao, and A. E. Suyker. 2015. Estimation and analysis of gross primary production of soybean under various management practices and drought conditions. ISPRS Journal of Photogrammetry and Remote Sensing 99:70–83.

Wang, W., J. Dungan, H. Hashimoto, A. R. Michaelis, C. Milesi, K. Ichii, and R. R. Nemani. 2011. Diagnosing and assessing uncertainties of terrestrial ecosystem models in a multimodel ensemble experiment: 1. Primary production. Global Change Biology 17:1350–1366.

Wu, C., J. M. Chen, and N. Huang. 2011. Predicting gross primary production from the enhanced vegetation index and photosynthetically active radiation: evaluation and calibration. Remote Sensing of Environment 115:3424–3435.

Xiao, X., D. Hollinger, J. Aber, M. Goltz, E. A. Davidson, Q. Zhang, and B. Moore Iii. 2004. Satellite-based modeling of gross primary production in an evergreen needleleaf forest. Remote Sensing of Environment 89:519–534.

Xiao, X., S. Boles, J. Liu, D. Zhuang, S. Frolking, C. Li, W. Salas, and B. Moore. 2005. Mapping paddy rice agriculture in southern China using multi-temporal MODIS images. Remote Sensing of Environment 95:480–492.

Yan, H., Y. Fu, X. Xiao, H. Q. Huang, H. He, and L. Ediger. 2009. Modeling gross primary productivity for winter wheat–maize double cropping system using MODIS time series and CO_2 eddy flux tower data. Agriculture, Ecosystems & Environment 129:391–400.

Yuan, W., S. Liu, G. Zhou, G. Zhou, L. L. Tieszen, D. Baldocchi, C. Bernhofer, H. Gholz, A. H. Goldstein, and M. L. Goulden. 2007. Deriving a light use efficiency model from eddy covariance flux data for predicting daily gross primary production across biomes. Agricultural and Forest Meteorology 143:189–207.

Zeng, N., F. Zhao, G. J. Collatz, E. Kalnay, R. J. Salawitch, T. O. West, and L. Guanter. 2014. Agricultural Green Revolution as a driver of increasing atmospheric CO_2 seasonal amplitude. Nature 515:394–397.

Zhang, Q., X. Xiao, B. Braswell, E. Linder, F. Baret, and B. Moore. 2005. Estimating light absorption by chlorophyll, leaf and canopy in a deciduous broadleaf forest using MODIS data and a radiative transfer model. Remote Sensing of Environment 99:357–371.

Zhang, Q., E. M. Middleton, H. A. Margolis, G. G. Drolet, A. A. Barr, and T. A. Black. 2009. Can a satellite-derived estimate of the fraction of PAR absorbed by chlorophyll (FAPAR chl) improve predictions of light-use efficiency and ecosystem photosynthesis for a boreal aspen forest? Remote Sensing of Environment 113:880–888.

Zhang, Y., L. Guanter, J. A. Berry, J. Joiner, C. Tol, A. Huete, A. Gitelson, M. Voigt, and P. Köhler. 2014. Estimation of vegetation photosynthetic capacity from space-based measurements of chlorophyll fluorescence for terrestrial biosphere models. Global Change Biology 20:3727–3742.

Data Availability

Data associated with this paper have been deposited in Dryad: http://dx.doi.org/10.5061/dryad.64n47